47th AIAA Aerospace Sciences Meeting Including The New Horizons Forum and Aerospace Exposition
5 - 8 January 2009, Orlando, Florida

AIAA 2009-905

47th AIAA Aerospace Sciences Meeting Including The New Horizons Forum and Aerospace Exposition, 5-8 Jan 2009, Orlando, Florida

Asymmetry Features Independent of Roll Angle for Slender Circular Cone

Xuanshi Meng*, Zhide Qiao†, Chao Gao‡
Northwestern Polytechnical University, Xi'an 710072, China
Shijun Luo§, and Feng Liu¶
University of California, Irvine, CA 92697-3975

Based on a comprehensive low-speed pressure-measurement data for a cone of semi-apex angle 10° over whole roll angle range at high angles of attack up to 35°, the present paper shows that there exist asymmetry features which are independent of roll angle and, thus, applicable to models having the same geometry specifications. Verifications are made by comparing with available experimental data in literature. Mechanisms for the asymmetric-force features are identified.

Nomenclature

C_n	=	yawing-moment coefficient about cone base, yawing moment/$q_\infty SD$
C_p	=	pressure coefficient
C_{Yd}	=	local side force coefficient, local side force/$q_\infty d$
C_{Y0}	=	overall side force coefficient, overall side force/$q_\infty S$
D	=	base diameter of circular cone
d	=	local diameter of circular cone
L	=	length of circular cone
q_∞	=	free-stream dynamic pressure
Re	=	Reynolds number based on D
α	=	angle of attack
θ	=	meridian angle measured from windward generator, positive when clockwise
ϕ	=	roll angle, positive when clockwise

I. Introduction

The most interesting phenomena associated with high angle of attack aerodynamics is the asymmetry onset for slender body of revolution in symmetric flight. The lateral forces vary with roll angle dramatically. The variation trends depend on the micro surface imperfections of the test model, and thus are different for different models with the same geometry specifications. Much of experimental work has been spent on understanding and predicting the complicated force-asymmetry.

From a pressure measurements on a circular cone of semi-apex angle 10° at low speeds,[1] Fiddes[2] illustrated that for a front pressure station on the cone and angle of attack of 35° the maximum positive and maximum negative local side forces over the whole range of roll angle have the same magnitude, and are associated with

*Graduate Student, Department of Fluid Mechanics.
†Professor, Department of Fluid Mechanics.
‡Professor and Associate Director, Aerodynamic Design and Research National Laboratory.
§Researcher, Department of Mechanical and Aerospace Engineering.
¶Professor, Department of Mechanical and Aerospace Engineering. Associate Fellow AIAA.

a characteristic circumferential pressure distribution that is independent of roll angle, apart from a change of hand. There are some intermediate side forces between the maximum positive and maximum negative local side forces. Luo[3] conjectured that the local side force and pressure association may also hold true for the intermediate local side forces. Recently, Jia et al.[4] confirmed the conjecture using the measured pressures obtained under about the same test conditions of Fiddes. The present paper will investigate the detailed relationship between the local side force and pressures for a range of angle of attack and over the whole length of cone forebody.

Pidd and Smith[5] using the same experimental data[1] found that at angle of attack of 35° the local side-force lengthwise variation indicates a predominant conical flow to appear, but at 30° it only occurs exceptionally. We will attempt to further the examination.

The objectives of this paper are to further the insights into the local side-force variations with roll angle for slender circular cone at high angles of attack, and to establish the asymmetry features independent of roll angle. The present study is based on a comprehensive pressure measurements over a 10° cone by Meng et al.[6]

In the following sections, the experimental setup and results are briefly reviewed. The variation of local side force with roll angle at various angle of attack calculated from the measured pressures are presented. The asymmeric-force characteristics which is independent of micro surface imperfections of the models are presented and discussed. Lastly, conclusions are offered.

II. Experimental Setup

The tests were conducted in the 3.0×1.6 m wind tunnel at the Aerodynamic Design and Research National Laboratory, Northwestern Polytechnical University. The tunnel has a free-stream turbulence level of 0.045%. The angle of attack $\alpha = 0° - 35°$. The free-stream velocity is 30 m/s. The Reynolds number based on the cone base diameter $Re = 0.3 \times 10^6$.

The model is rigidly supported in the test section as shown in Fig. 1. A thorough job of cleaning the model surface was done prior to each run of the wind tunnel.

The model comprises a circular cone of 10° semi-apex angle faired to an after cylinder. The model is made of metal and constructed to an average tolerances of ± 0.05 mm with a surface finish of nearly ± 0.8 μm. The model forebody is fixed to the shaft of a step motor and can be rolled through 360°. The junction between the forebody and the after cylinder is carefully machined so that the surface discontinuity is less than 0.025 mm.

The pressure instrumentation is confined to the cone and is well forward of the model supports. The pressure tappings are uniformly distributed at 9 stations along the cone length from $x/L = 0.212$ to 0.813 as shown in Fig. 1. Stations 1 and 2 have 12 and 18 pressure orifices, respectively, and the rest stations have 36 pressure orifices. The pressure orifices in each station are equally-spaced around the circumference and arranged from the same datum for all stations.

The static pressure at the each pressure orifice is transmitted by a rubber tube passing through the base of the afterbody to the pressure-measurement system outside the test section. The system consists of 24 scan-valves each of which has 16 channels and one pressure transducer of modulus 9816 made by the PSI Company with an accuracy of ±0.05%. The pressure measurement readings for each test case were taken 115 times in 0.05 *sec* intervals and then time-averaged. The time-averaged results show the hoped-for steady flow. The time-averaged pressure distributions are documented in Ref. 6. No flow field surveys were made in the present tests.

III. Base Plasma-Off Flow at Zero Angle of Attack

The experimental setup is verified by measured pressures at zero angle of attack. Figure 2 presents the pressure coefficient c_p versus θ at $\alpha = 0°$ and $\phi = 0$ for all stations. The maximum variation of c_p with θ is generally less than 0.01 on each station except the two front stations. The maximum variation of 0.2 on Station 2 at $\theta = 350°$ may be caused by an uncareful handling of the model. Figure 3 presents the pressure coefficient c_p at Orifice 1 versus ϕ at $\alpha = 0°$ for all stations. Orifice 1 is located at $\theta = 230°$ when $\phi = 0°$. The maximum variation of c_p with ϕ is also smaller than 0.01 on all stations. Figs. 2 and 3 verify that the model is axi-asymmetric and the model axis parallels with the free-stream velocity at zero angle of attack

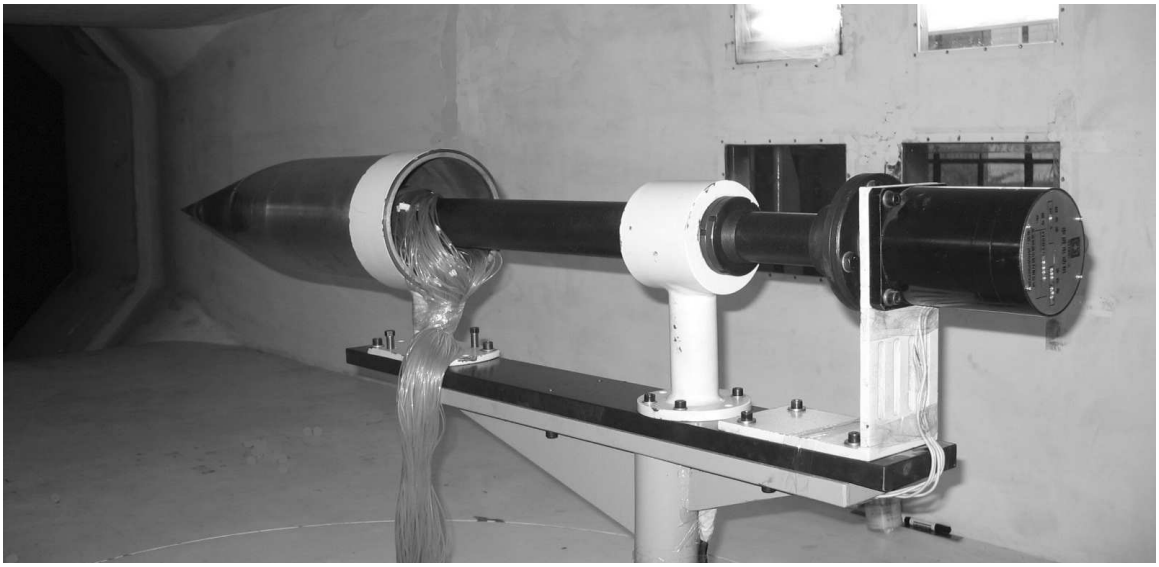

(a) model in the wind tunnel

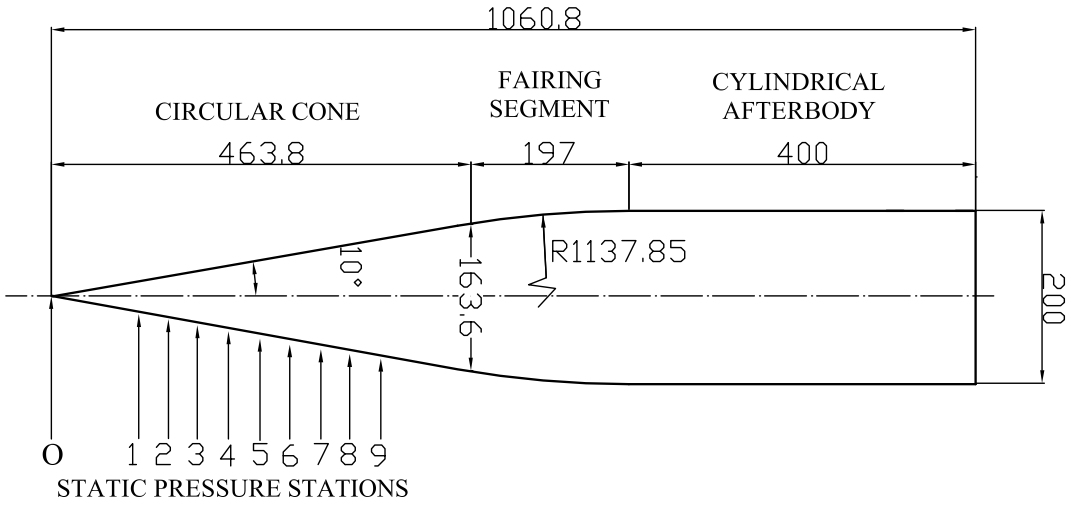

O—1	O—2	O—3	O—4	O—5	O—6	O—7	O—8	O—9
98.5	133.2	166.8	201.9	236.9	272.0	307.1	342.1	377.2

DIMENSIONS IN mm

(b) the model

Figure 1. The model in the wind tunnel.

for all roll angles.

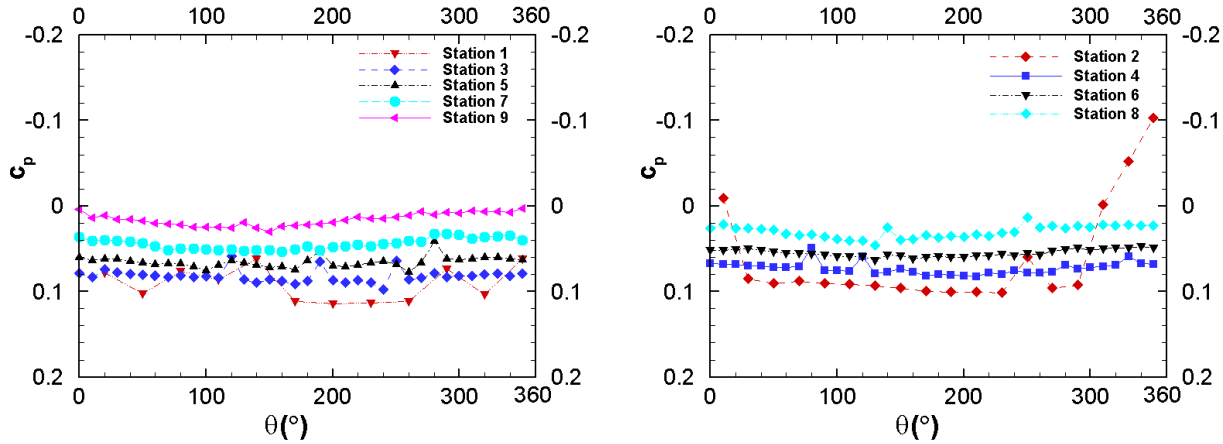

(a) Odd-numbered stations (b) Even-numbered stations

Figure 2. Pressure coefficient vs. θ at $\alpha = 0°$ and $\phi = 0$.

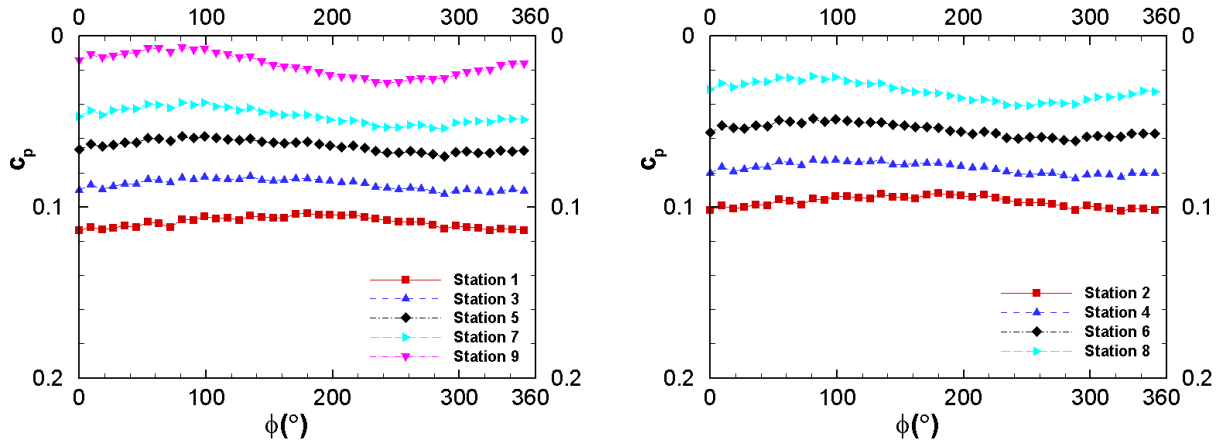

(a) Odd-numbered stations (b) Even-numbered stations

Figure 3. Pressure coefficient vs. ϕ at $\alpha = 0°$ and Orifice 1.

IV. Variation of Local Side-force Coefficient with Roll Angle

The local side forces are calculated from the measured pressures and normalized by the local diameter, d of the cone rather than the base diameter D, in order to confer more information as shown by Hall.[7] Figure 4 presents the local side-force coefficient (positive when sideslip to the starboard side) versus roll angle at various angles of attack for the odd-numbered stations. The results for even-numbered stations are similar.

When angle of attack is increased to double semi-apex angle of the cone asymmetry onsets, and when increased to about triple semi-apex angle the local side-force variation with roll angle changes from continuous-wave curve to square-wave curve. The continuous-wave curve indicates that the asymmetry at a given angle of attack has multple bi-stable patterns of different amplithdes dependent of the micro surface imperfections of the model at different roll angle. The square-wave curve indicates that the asymmetry at a given angle of attack has mainly one bi-stable pattern of an extreme amplitude for the model at various roll angle.

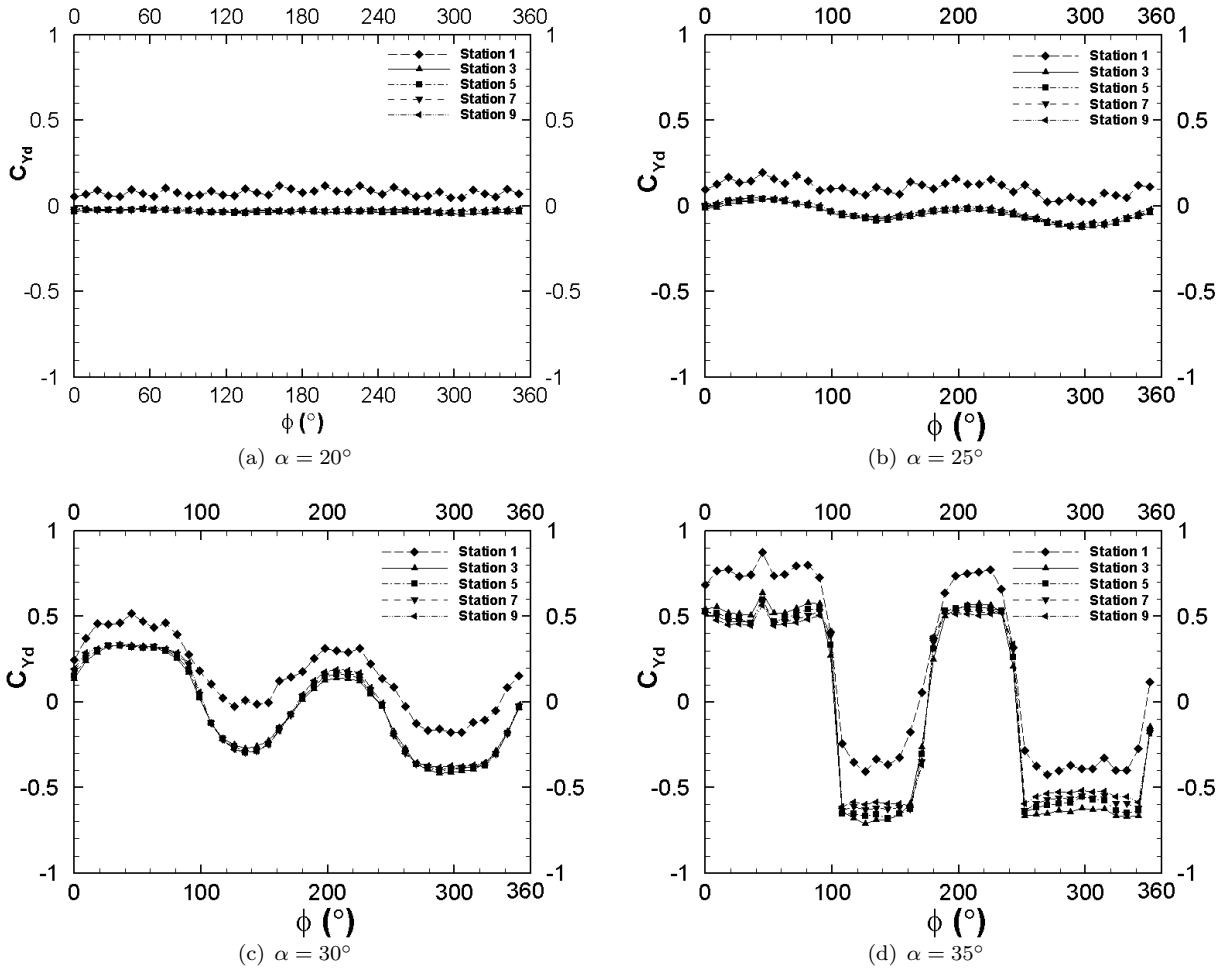

(a) $\alpha = 20°$ (b) $\alpha = 25°$

(c) $\alpha = 30°$ (d) $\alpha = 35°$

Figure 4. Local side-force coefficient vs. roll angle for odd-numbered stations.

V. Conicity of Pressure Distributions

Figure 5 presents the pressure coefficients on six meridian lines in 60° intervals versus longitudinal coordinate, x/L at $\phi = 171°$ for $\alpha = 20° - 35°$. The pressures are almost constant over the measured Stations 3 through 9 ($x/L = 0.340 - 0.813$) and, thus, the flow is essentially conical. The pressures are asymmetric starting from the apex of the body. C_{Yd} approaches a non-zero value as x approaches zero, since the local side force coefficient C_{Yd} is normalized by the local diameter d. This is true for all roll angles.

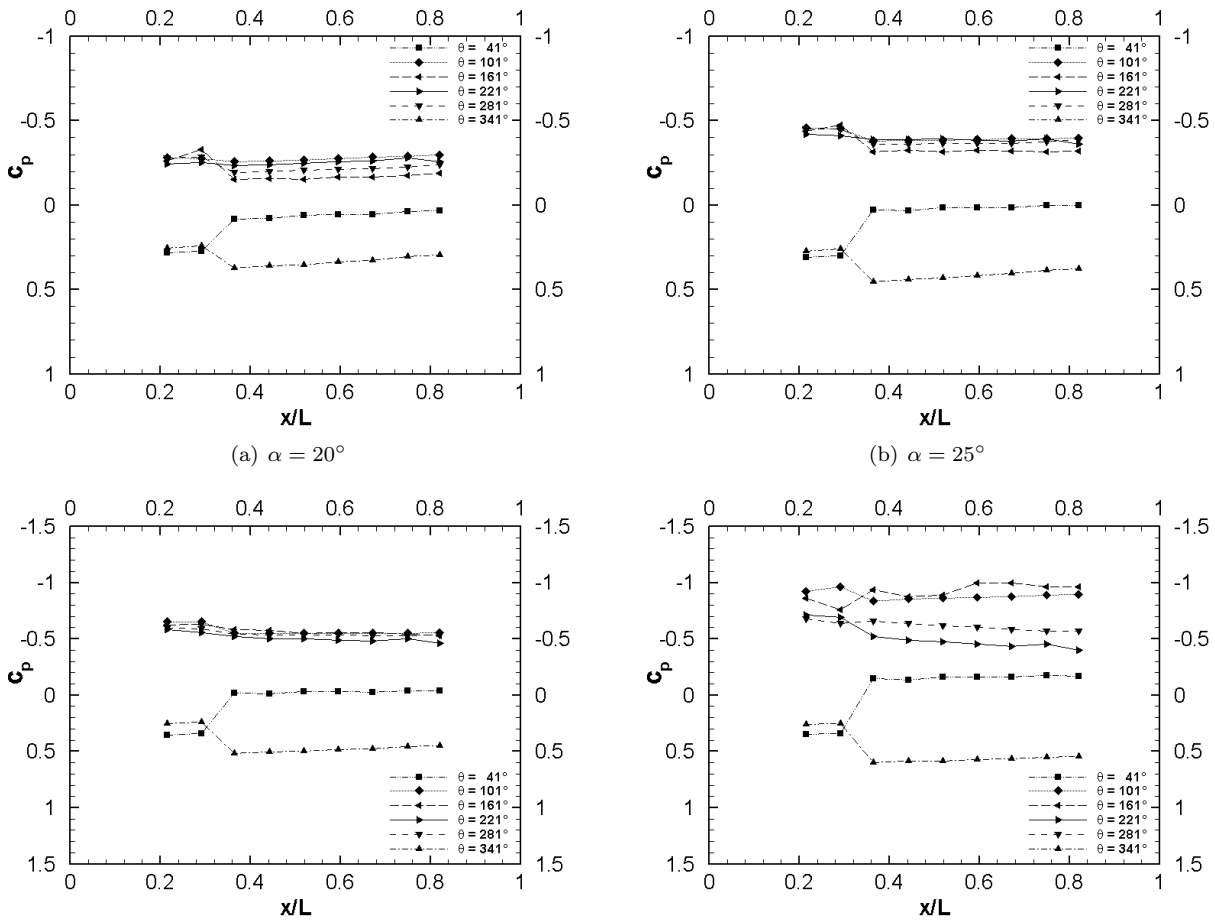

(a) $\alpha = 20°$ (b) $\alpha = 25°$

(c) $\alpha = 30°$ (d) $\alpha = 35°$

Figure 5. Pressure coefficient vs. x/L at various θ and $\phi = 171°$.

VI. Maximum Side Force and Yawing Moment

For a given angle of attack, the magnitudes of the maximum positive side force and maximum negative side force coefficients over the whole range of roll angle are nearly equal, called extreme magnitude of the local side-force coefficient $|C_{Yd,max}|$. The small deviations may be attributed to micro asymmetries in the experimental setup. Table 1 compares the extreme local side-force coefficient, $|C_{Yd,max}|$ of the present model with that obtained from the model of Ref. 1 for $\alpha = 30°$ and 35° given by Pitts et al.[5] and Fiddes,[2] respectively, which have been corrected by a factor of 2 for a possible difference in the local side-force coefficient definition. Taking the correction for grant, the extreme magnitude of the local side-force coefficients are equal for different models with the same geometry specifications.

Table 1. Comparison of $|C_{Yd,max}|$ of the present model with that of the model of Ref. 1.

α	$\lvert C_{Yd,max}\rvert$	
	Present model	Model of Ref. 1
30°	0.33	0.65/2
35°	0.55	1.10/2

Figure 6 presents the maximum and minimum values of the overall side-force and yawing-moment coefficients versus angle of attack and a comparison with the force-measurement results of Keener et al.[8] The latter results were measured at one roll angle and lie between the present maximum and minimum curves, which confirms that the maximum and minimum are independent of the micro surface imperfections of the models. The magnitudes of the maximum and minimum values are approximately equal.

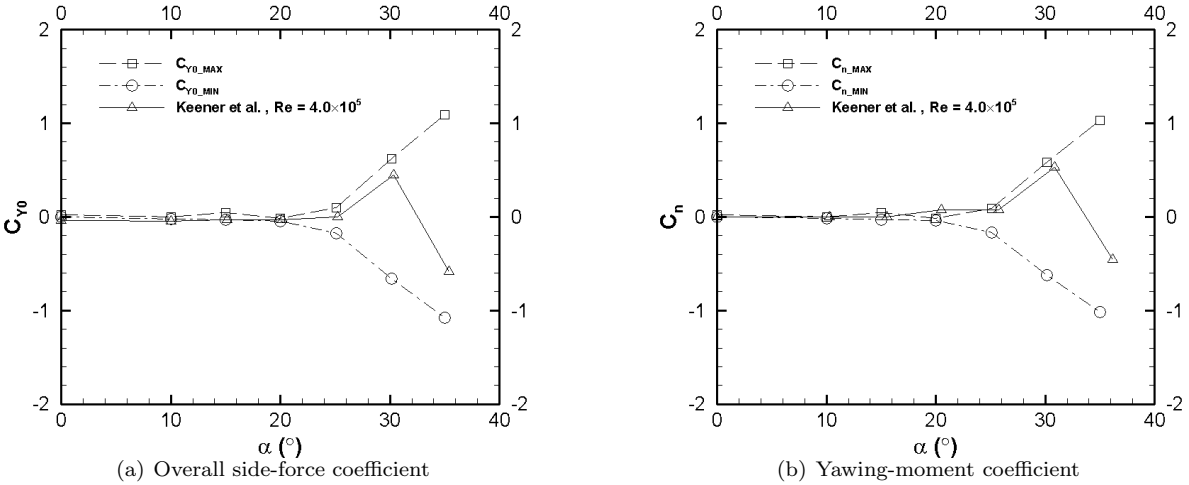

(a) Overall side-force coefficient

(b) Yawing-moment coefficient

Figure 6. Maximum and minimum of overall side-force and yawing-moment coefficients vs. α compared with Keener et al.[8]

VII. Pressure Distributions Giving Equal Local Side Force

The local side force depends on the roll angle of the model. However, the pressure distributions corresponding to equal local side force are independent of roll angle. This is true for all angles of attack. A number of judiciously chosen cases are considered. Take any two points from the wave curve of $C_{Yd}(\phi)$ for a given station, which give local side force of equal magnitudes with either same or opposite sign and compare the corresponding pressure distributions.

A. At $\alpha = 25°$

Two cases are chosen from the curve $C_{Yd}(\phi)$ at $\alpha = 25°$ and Station 3 from Fig. 4. Fig 7 compares the pressure distributions for the two cases. The pressures are identical for each case.

B. At $\alpha = 30°$

For $\alpha = 30°$, Two cases are chosen from Fig. 4 at Station 1. Their pressure distributions are identical for each case as shown in Fig. 8.

Two cases are chosen at Station 3, $\alpha = 30°$ and the pressure distributions are compared in Fig. 9. In each case the pressure distributions are identical. Another two cases having C_{Yd} almost equal to zero are shown in Fig. 9. The pressure distributions not only coincide but also are symmetric with respect to the incidence plane of the model.

Two cases are chosen from Station 9, $\alpha = 30°$ and the pressure distributions are compared in Fig. 10. For the first case the pressure distributions are identical. For the second case the local side forces are of

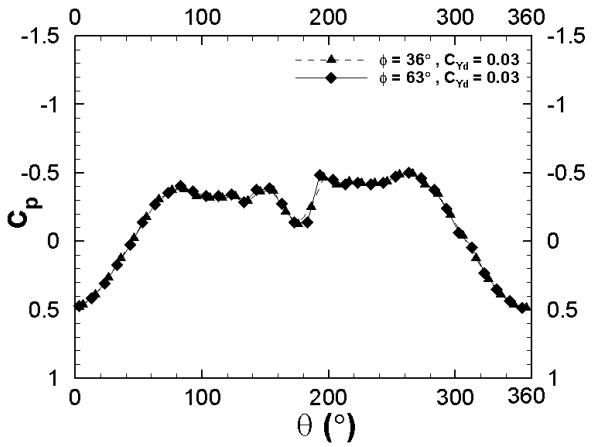

(a) $C_{Yd} = 0.03$

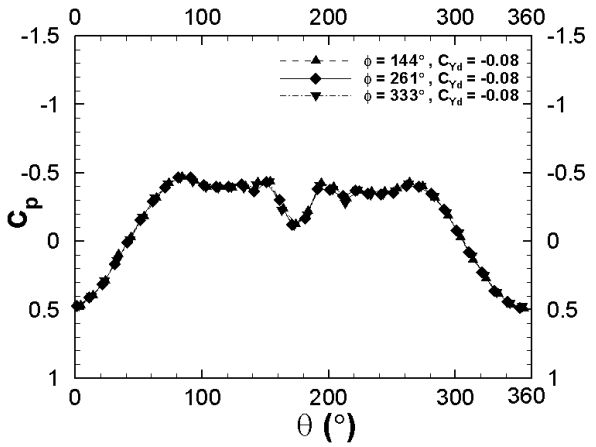

(b) $C_{Yd} = -0.08$

Figure 7. Comparison of pressure distributions corresponding to equal local side force at Station 3, $\alpha = 25°$.

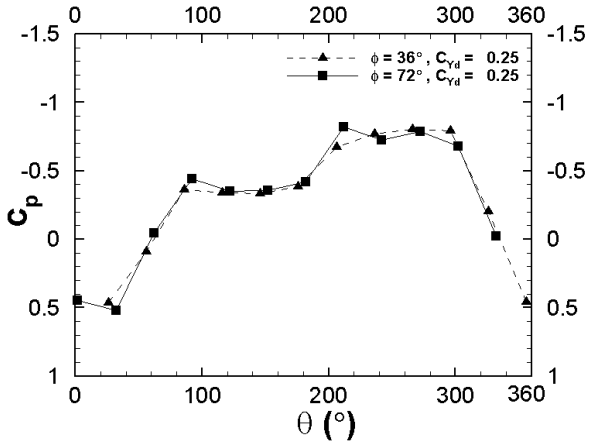

(a) $C_{Yd} = 0.25$

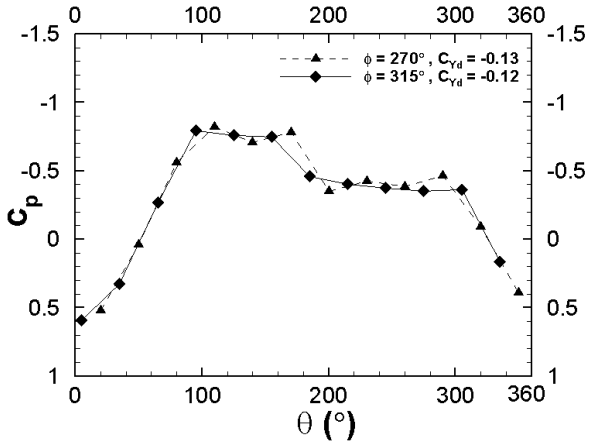

(b) $C_{Yd} \approx -0.12$

Figure 8. Comparison of pressure distributions corresponding to equal local side force at Station 1, $\alpha = 30°$.

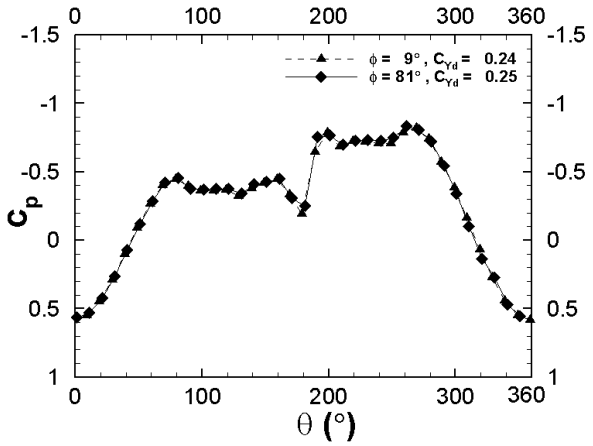

(a) $C_{Yd} = 0.24$

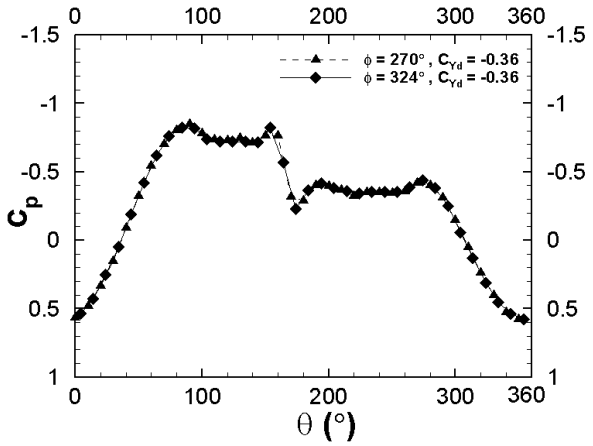

(b) $C_{Yd} = -0.36$

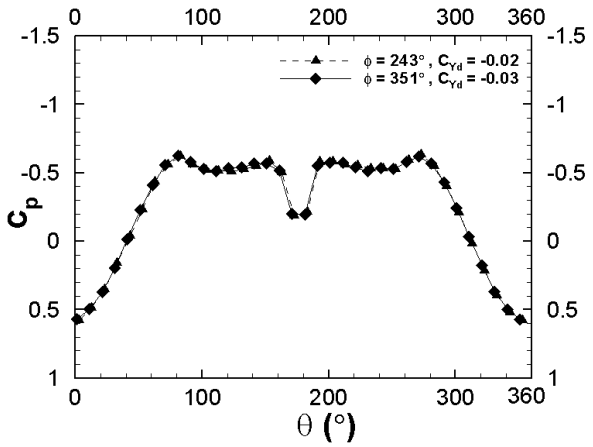

(c) station 3, $C_{Yd} \approx -0.02$

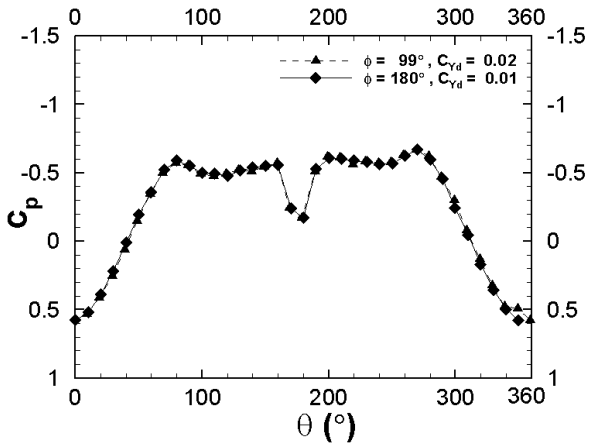

(d) station 3, $C_{Yd} \approx 0.02$

Figure 9. Comparison of pressure distributions corresponding to equal local side force at Station 3, $\alpha = 30°$.

equal magnitude but opposite sign and the pressure corresponding to the negative C_{Yd} is plotted versus $(360° - \theta)$. The slight deviation between the two pressure distributions is brought about by changing hand in plotting one of the two pressures, and may be caused by inaccuracy of the roll-angle setting.

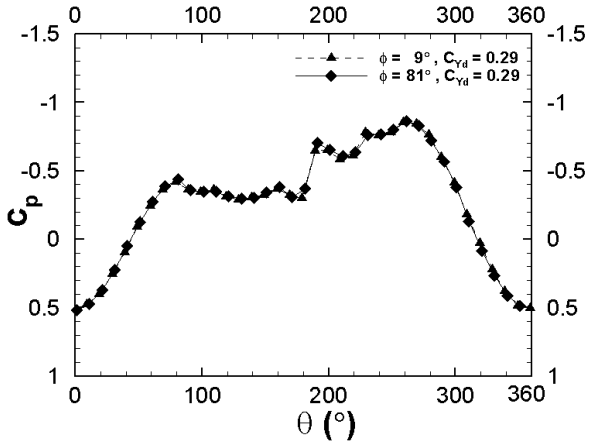

(a) $C_{Yd} = 0.29$

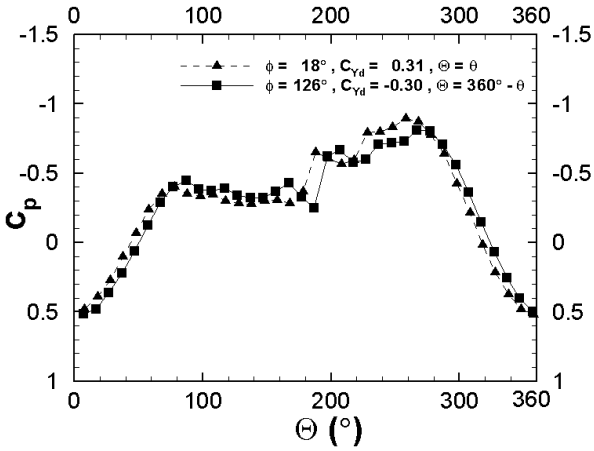

(b) $C_{Yd} \approx \pm 0.30$

Figure 10. Comparison of pressure distributions corresponding to equal local side force at Station 9, $\alpha = 30°$.

C. At $\alpha = 35°$

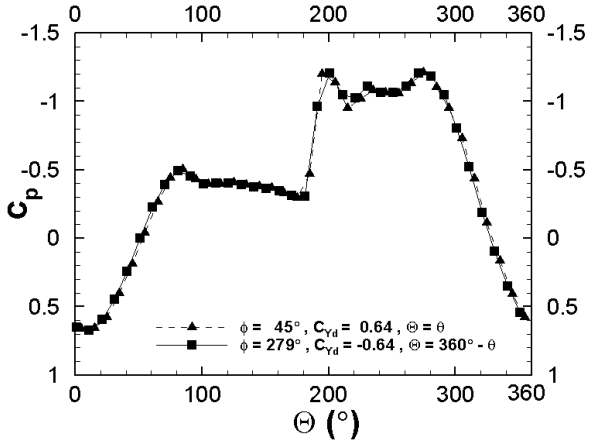

(a) $C_{Yd} = \pm 0.64$

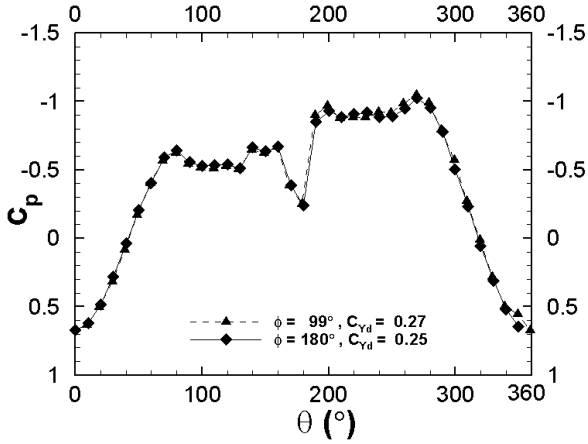

(b) $C_{Yd} \approx 0.25$

Figure 11. Comparison of pressure distributions corresponding to equal local side force at Station 3, $\alpha = 35°$.

For $\alpha = 35°$, two cases are chosen from Fig. 4 at Station 3. The pressure distributions are compared in Fig. 11. For the first case the pressure distributions are identical. For the secomd case the local side forces are of equal magnitude and opposite sign and the pressure corresponding to the negative C_{Yd} is plotted versus $(360° - \theta)$. They are almost identical.

VIII. Comparison with Model of Ref. 1

Figure 12 compares the pressure distribution with that given by Fiddes[2] under about the same test conditions. Both models are of 10° semi-apex angle and tested at $\alpha = 35°$, and low speeds. The positions of the pressure-measuring station and the free-stream Reynolds numbers are close to each other as shown in the figure. Both pressures give the same maximum local side force. The roll angle of the present model is

chosen at 342° for the matching.

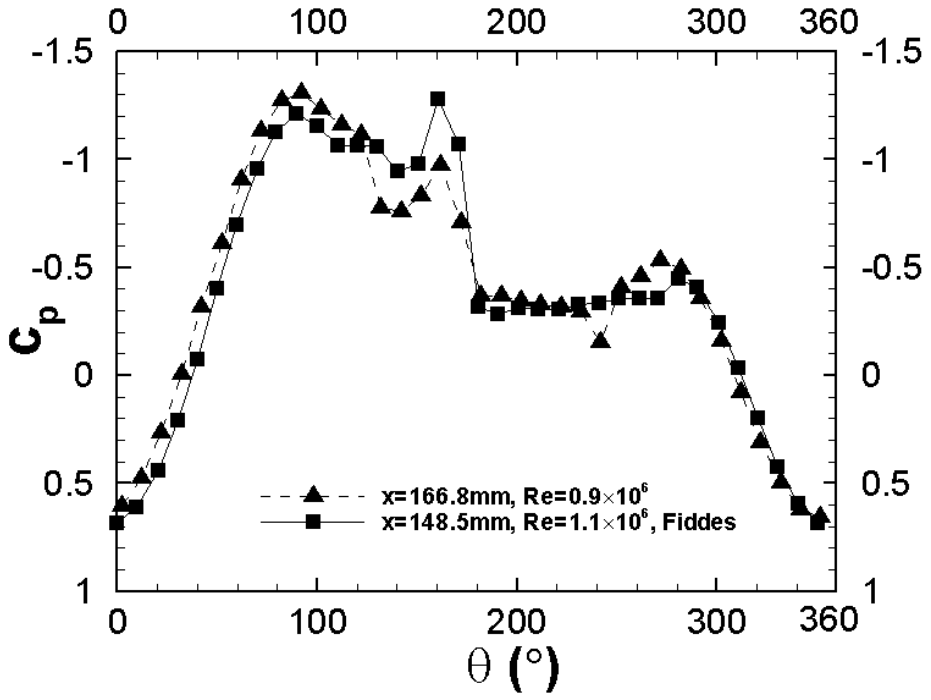

Figure 12. Pressure distribution at Station 3, $\phi = 342°$ compared with Fiddes' result[2] at $\alpha = 35°$.

The pressure distributions are nearly identical. A minor deviation may be caused by different separation states of the boundary layer. The primary state of boundary layer can be inferred from the measured pressures.[9] Fiddes' pressure distribution indicates a laminar separation on the starboard side and a laminar bubble separation followed by a turbulent re-attachment and a turbulent separation, i.e., a transitional separation on the port side of the pressure station. The present pressure distribution indicates a turbulent separation on the both sides at the pressure station. The differences of the boundary-layer state are attributed to the different micro surface imperfections of the two models and the different free-stream turbulence levels of the two wind tunnels.

Hence, every local side-force coefficient is associated with a characteristic circumferential pressure distribution which is independent of roll angle (or micro surface imperfections of the model), apart from a change of hand. For zero local side force the pressure distributions are symmetric to the incidence plane of the model. Asymmetric pressure distributions occur in pair. They are mirror images to each other. The existence of mirror-imaged pressures indicates that the asymmeric force is produced by the leeward-side asymmetric-vortex configurations.

IX. Conclusions

The study of the pressure measurement data over a slender circular-cone forebody at high angles of attack up to 35° shows that there exist asymmetry features which are independent of roll angle and, thus, applicable to models of the same geometry specifications.

1. The distributions of pressure and local side-force coefficient coefficient (normalized by local diameter of the cone) over the main portion (except the apex and the base region) of the conical forebody are conical at all angles of attack, even though the wind speed is subsonic. Force asymmetry starts right at the apex of forebody.

2. The magnitudes of maximum positive and maximum negative local side force coefficient are equal over the conical forebody at given angle of attack.

3. The circumferential pressure distributions giving equal local side force coefficient over the conical forebody are identical at given angle of attack.

The asymmetric force is mainly produced by the leeward-side asymmetric vortex configurations which, in turn, is a result of an instability mechanism, while the boundary-layer states may have minor effects.

Acknowledgments

The present work is supported by the Foundation for Fundamental Research of the Northwestern Polytechnical University, NPU-FFR-W018101. The authors are grateful to Professor Xueying Deng of Beijing University of Aeronautics and Astronautics for using the pressure-transducer system.

References

[1]Fiddes, S.P. Lean, D.E., and Moir, I.R.M., "Experimental investigation of the separated flow past slender bodies in the RAE 5 metre low-speed pressurised wind tunnel," RAE Publication, unavailable to the present authors.

[2]Fiddes, S., "Separated flow about cones at incidence–theory and experiment," *Proceedings of Symposium on Studies of Vortex Dominated Flow*, NASA/LRC, 1985, pp. 285–310.

[3]Luo, S., "Asymmetric vortex flow over slender bodies," *Proceedings of Conference on New Century Mechanics*, Beijing, Nov. 2001, pp. 198–205.

[4]Jia, C., Meng, S., Qiao, Z., Gao, C., Luo, S., and Liu, F., "Pressure around a 20-degree circular cone at 35-degree angle of attack and low speed," AIAA Paper 2007-4453, June 2007.

[5]Pidd, M. and Smith, J., "Asymmetric vortex flow over circular cones," *Vortex Flow Aerodynamics, AGARD CP-494*, July 1991, pp. 18–1–11.

[6]Meng, S., Jia, C. ,Qiao, Z., Gao, C., Luo, S., and Liu, F., "Development of flow asymmetry over a 20-degree circular cone at low speed," AIAA Paper 2007-4118, June 2007.

[7]Hall, R.M., "Forebody and missile side forces and the time analogy," AIAA-87-0327, Jan. 1987

[8]Keener, E., Chapman, G., Cohen, L., and Taleghani, J., "Side forces on Forebodies at high angles of attack and Mach numbers from 0.1 to 0.7: two tangent ogives, paraboloid and cone," NASA TM X-3438, Feb. 1977.

[9]Hall, R.M., "Influence of Reynolds number on forebody side forces for 3.5-diameter tangent-ogive bodies," AIAA-87-2274, Jun. 1987